City Research Online

City, University of London Institutional Repository

This is the accepted version of the paper.

This version of the publication may differ from the final published version.

Head Phantom Optical Properties Validation for Near-Infrared Measurements: A Comparison with Animal Tissue

M. Roldan and P. A. Kyriacou, *Senior Member, IEEE*

Abstract— The interest in optical healthcare technologies has increased significantly over the recent years. The innovation of new optical technologies such as Near Infrared Spectroscopy (NIRS), used for the monitoring of brain perfusion, demands a comprehensive understanding and knowledge of the light tissue interaction. Phantoms can provide a rigorous, reproducible and convenient approach for evaluating an optical sensor's performance. However, up to date literature does not provide a detailed description of a complete head model that involves the human anatomy, physiological changes, and the tissue optical properties. The latter is key for the design, development and testing of optical sensors, such as NIRS technologies. This paper compared the optical properties of the materials chosen to build a head phantom, against the optical properties of real brain and skull tissues extracted from animal models. The spectra of a silicone brain and resin skull samples were compared with the spectra of the respective tissues extracted from pigs and mice. The results of this study demonstrated that both phantom materials have similar optical properties to mice and pigs' tissues. The morphology of the phantom's spectra were very similar to the respective animal tissue comparator.

I. INTRODUCTION

The interest of optical technologies in healthcare has increased substantially in the last century. The reported applications of photoplethysmography (PPG) and Near-Infrared Spectroscopy (NIRS) in the recent years have been most impressive. Since 1977, when NIRS was first described for monitoring cerebral perfusion and brain oxygenation [1], clinical implementation of this optical technology has increased [2]. For instance, tissue oxygenation has become increasingly common for cerebral oxygenation monitoring of preterm children [3]. Similarly, active cerebral monitoring with NIRS oximeters has an important impact during and after neurosurgery [3]. Nowadays, wearable devices also include optical sensors for oxygenation levels monitoring, heart frequency monitoring, among others.

Effective monitoring devices can decrease mortality and can improve neurological outcomes. Therefore, it is relevant to evaluate the performance of optical technologies, evaluating the light-tissue interaction within the light spectra and tissue of interest (e.g., the brain). Phantom-based performance tests for NIRS monitoring can provide a rigorous, reproducible and convenient approach to evaluating performance using well-characterized materials [3]. This in-vitro method enables well controlled experiments where multiple parameters can be set, such as anatomical characteristics (e.g., layers' thickness),

physiological changes (e.g., pressure, frequency, oxygen levels) or device design variables (e.g., illumination wavelengths, and optical sensor (source and detector) topology). A NIRS compatible head phantom would allow the simulation of different clinical scenarios that cannot be induced in healthy volunteers.

Previous NIRS phantoms were used for oximetry performance testing [3], [4]. The literature reported box models that mimicked the skull, filled with a rectangular silicone brain. The materials' optical properties weren't compared with real head tissues and only changes in blood oxygenation levels were simulated [3], [4]. However, in order to go forward in the development of more complete optical technology, a more complex head phantom is needed.

Traumatic brain injury (TBI) is, as its name indicates, an acquired head injury caused by an external force that disturbs the brain's function [5], [6]. TBI is among the most severe types of injury in terms of fatality and lifelong disability for survivors [7], [8]. Intracranial pressure (ICP) and cerebral oxygenation are the main biomarkers for assessing TBI [9] [10]. Unfortunately, both measurements require invasive interventions, increasing the risk of complications including haemorrhage or infection, and for this reason they are generally only implemented by neurosurgeons. Hence, delays on assessment and treatment are common causes of secondary injuries, increased mortality and worst outcomes [11]. Therefore, there is an unmet need in developing noninvasive techniques enabling the continuous monitoring of TBI, especially to assess brain's hemodynamic during the first hours after trauma, when secondary injury takes place [9], [12].

The future development of a NIRS multiparametric sensor for TBI monitoring requires a complete, well controlled, and optically compatible phantom. This set-up would be then a source of information during the design, development, and testing phases of the sensor. Therefore, the current study aims to compare the optical properties of the materials chosen to build a head phantom, against the optical properties of real brain and skull tissues extracted from animal models.

II. METHODS

A. Phantom samples

Artificial brain and skull tissues were developed in order to build a phantom that mimics the optical properties of real head tissues. The main goal is to assess the brain using near infrared light, which passes through the skull and reaches the

brain. In this phase of the research extracerebral perfusion was not included, hence the phantom lacks scalp.

The phantom brain sample (10 x 10 x 20 mm) was developed in silicone gel (Sylgard 527, DOWSIL – Dow Corning, Michigan, U.S.A) as this material resembles the mechanical properties of the brain under dynamic and static conditions [13], [14]. The casting mixture was prepared by adding two-part silicone gel in a ratio of 1:1 and, as the silicone gel is transparent with minimal scattering properties, Titanium Dioxide (TiO2) particles with a primary crystal size of 550 nm (Altiris 550, Venator Corporation, Teesside, UK) were added in the mixture in a ratio of (weight/volume) of 0.1 g/100 mL to simulate near-infrared scattering. The solution of Sylgard 527 and Titanium Dioxide particles was then hand-mixed and sonicated for ten minutes. The mix went into three vacuum chamber cycles before undergoing a degassing cycle of another 10 minutes (i.e. to remove air bubbles which may cause optical heterogeneities within the phantom). After an initial curing cycle in the oven of 4 hours at 125 °C temperature, the silicone phantom was removed from the casting and placed in the oven at 125 °C for one extra hour. Once the sample was at room temperature, it was placed in a UVette® plastic cuvette to protect the sample from any damage due to its adhesive texture.

The phantom skull sample (10 x 10 x 20 mm) was 3D printed in the Form 2 printer from Formlabs (Somerville,MA,USA), which uses a laser to cure solid isotropic parts from a liquid photopolymer resin. All standard Formlabs' resins have comparable material properties to those reported from the cranial bone. For instance, evidence reports a tensile strength of the human skull of 67.73Mpa, which is close enough to the tensile strength of the phantom's resin (65Mpa) [15]. Moreover, according to McElehaney the human skull elastic module ranges between 2.41 and 5.58 GPa, in comparison Formlabs resin has an elastic module of 2.8 GPa which is in the range reported by McElehaney [16]. However, other authors have found a higher value for the skull elastic module (mean: 8.51Gpa), therefore the phantom resin would be somewhat more compliant than actual cranial bone [17]. The phantom's resin was cured at 60ºC for 15 minutes in the UV chamber to get the recommended tensile modulus. To keep consistency between all the samples, it was also placed in a UVette® plastic cuvette.

B. Animal samples

Multiple animal models have been used in TBI research, yet rodents are most used due to its accessibility and low cost. The huge anatomical differences between rodents and humans have led to a greater interest in the assessment of large animal models, such as cats, dogs, sheep, pigs and monkeys [18]. Nonetheless, given the availability of mice and pigs' tissues, this study utilized brain and skull samples from both animal models. Five animals of each model were considered as tissue donors for this research, and only one sample of each tissue was extracted per animal. Thus, the animal samples were: 5 from mouse skull, 5 from mouse brain, 5 from pig skull and 5 from pig brain. Nevertheless, it is noteworthy to mention that pigs brain samples consist of 40% grey matter and 60% white matter, in contrast the whole brain of a mouse was contained in a single cuvette. Fig. 1 shows the brain and skull samples of the phantom materials from both animal models.
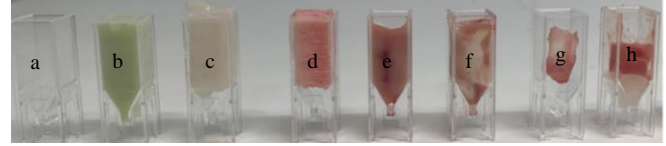

Fig.1. Empty cuvette reference (a), phantom skull with an optical path length (OPA) of 10 mm (b), phantom brain with OPA of 10 mm (c), pig skull with OPA of 8 mm (d), pig grey matter with OPA of 4 mm (e), pig white matter with OPA of 6 mm (f), mice skull with OPA of 1 mm (g) and mice brain with OPA of 5 mm (h).

C. NIR Spectroscopy

The spectra of the prepared samples were collected using a Lambda 1050 dual beam spectrophotometer from Perkin Elmer Corp. (Waltham, MA, USA). A 100 mm InGaAs integrating sphere detector set at 0 deg was used for detection of diffuse reflectance and diffuse transmittance measurements. For the animal test comparison, the spectra were acquired in the wavelength range and interval as the resin, yet the analysis was focused on the wavelength range between 700-880 which is the same band of wavelengths used in current NIRS devices. NIRS uses that wavelength because the absorption contribution of chromophores such as oxygenated and deoxygenated haemoglobin is maximized in this range, while the absorption contribution of other compounds such as water molecules is minimized [19].

Moreover, the Gain and Response Times for the spectrophotometer were maintained at 0 and 0.2 s, while both slit sizes were kept at 2 nm. These settings prevented the detectors from oversaturation. Reference beam attenuation was set at 100%, and UVette®disposable plastic cuvettes of 10 mm path length from Eppendorf® (Hamburg, Germany) were used. Also, for the acquisition of measurements in reflectance mode, a Spectralon Diffuse Reflectance Standard from Lapsphere (North Sutton, NH, USA) was placed at the aperture of the sphere detector for both baseline corrections and sample spectra collections. In this technique, one spectrum was produced per scan and three cycles were collected from each sample, which later were averaged to obtain a 23 spectra dataset.

Spectra collection and visualisation was performed using the software packages: UVWin Lab for LAMBDA 1050, from Perkin Elmer (Waltham, MA, USA). Further pre-processing of the spectra was in MATLAB R2019b, MathWorksTM (Natick, MA, USA) and the statistical analysis was carried out in IBM® SPSS® Statistics 26.0 (Armonk,NY,USA).

D. Data analysis

Due to the differences in size of the brain and skull of the mice and pigs, most of the samples had different

thicknesses (d) which might be a confounder in transmittance (T%) analysis as this implies different optical path lengths. A way to circumvent this issue is to compute the absorption coefficients (μ_a) for the assessed wavelength range; this coefficient relates both percentage of transmittance and the sample's thickness as shown on Equation 1.

$$\mu_a = \frac{\ln\left(\frac{100}{T\%}\right)}{d} \qquad [1]$$

Linear regression was calculated, as it gives important information about the differences and similarities of the two spectra. For instance, the coefficient of determination (R2), is a measure of the spectral similarity in terms of peak positions and relative intensities. Likewise, the slope of the regression (standardized beta coefficient) is a measure of the baseline corrected absorption intensities, thus a slope significantly different from one indicates differences in spectral features, and extra or missing peaks. Finally, the intercept of the regression line (constant) is a measure of any baseline offset between the spectra, in consequence a value far from 0 indicates an offset between compared spectra baselines might be related to scattering or cell effects. In conclusion, for a high quality match of spectra the expected coefficient of determination and the slope should be near to 1 and the intercept near to 0 [20].

III. RESULTS AND DISCUSSION

Transmittance is the proportion of the incident light that moves completely throughout the sample and is related to its optical path length. The absorption coefficients within the wavelength range were calculated to allow the comparison between the optical properties of the samples (Fig. 2).

The phantom brain absorption coefficients did not differ from the animal models' brain absorption coefficients, within the assessed wavelength range. Moreover, the absorption coefficients of the phantom skull laid in between the mice and

pigs' absorption coefficients, where the phantom and pigs' spectra were similar. These observations were corroborated by bivariate linear regression analyses presented in Table 1.

Table 1: Bivariate linear regression parameters for the absorption coefficients

Sample	R^2	Beta	Alpha
Mice brain	1	1	-2.49E-05
Pig brain	1	1	9.04E-07
Mice skull	0.995	0.998	0.0
Pig skull	0.992	0.996	0.0

On the other hand, the spectra on reflectance mode were not related to the sample's thickness, as reflectance is the proportion of incident light that is reflected from the tissue. In this case a small consideration was taken with pig brain samples, as the tissue contained both grey and white matter, hence the spectrophotometer test was run at both sides of the pig's brain samples. The mean reflectance spectra of the assessed samples are shown in Fig. 3.
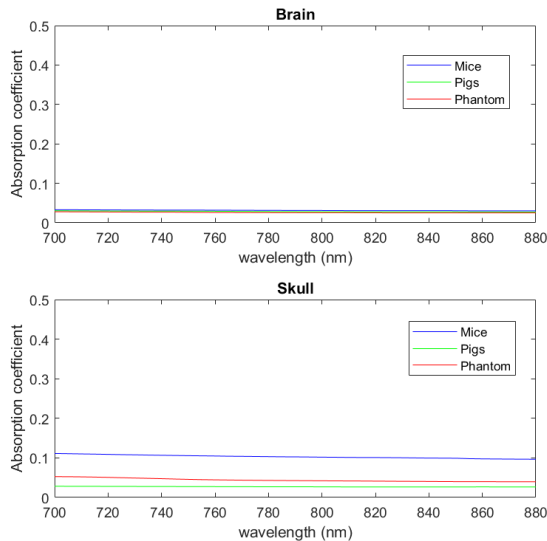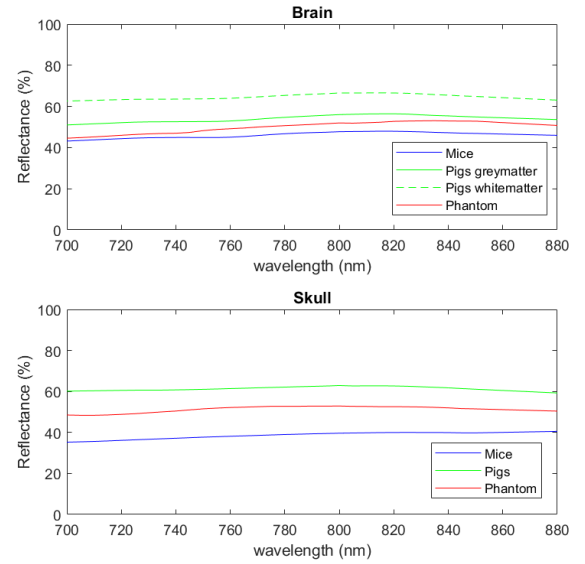

Fig. 3. Mean reflectance spectra within the range of 700 to 880 nm.

The proportion of incident light that was reflected from the phantom tissues laid in between the mice and pigs' spectra of both brain and skull samples. The phantom brain spectrum was closer to the pigs' grey matter spectrum, similarly the phantom skull reflected light barely changes within the spectra range. The mean reflected light of the phantom skull was 50% while the pig's mean reflected light was 10% more.

Fig. 2. Mean absorption coefficients within the range of 700 to 880 nm.

Table 2: Bivariate linear regression parameters for the reflectance spectra.

Sample	R^2	Beta	Alpha
Mice brain	1	1.086	-0.01
Pig grey matter	0.99	0.925	-0.01
Pig white matter	0.998	0.774	-0.007
Mice skull	0.99	1.326	0.022
Pig skull	1	0.837	-0.003

According to the results presented in Tables 1 and 2 the absorption coefficients and the percentage of reflectance spectra have the same morphology between the phantom materials and the animal tissues. Taking into account that R2 and Beta are almost 1 in all the comparisons and the value of Alpha is very closer to zero, which means that there are not significant differences on the peak's positions, the relative intensities, the spectra baselines or the offsets.

Some of the limitations of this study are as follows. Firstly, the animal models were mainly selected by the availability of the tissues, yet in order to have more accurate results, it would be interesting to reproduce this study with real human tissues. Nevertheless, the obtained absorption coefficients are not far from those reported in the evidence. For instance, Bevilacqua found an absorbance coefficient $<0.01\pm0.01$ mm^{-1} from the frontal lobe cortex of a healthy human brain tissue. The same author reported an absorbance coefficient of 0.05 ± 0.02 mm^{-1} in a healthy human skull, both measurements made between 674 and 954nm [21]. Secondly, the amount of data depended on the quality and number of animals available to be studied. Stronger analysis could have taken place with a bigger sample size, such as principal component analysis. Thirdly, the reproducibility and comparability of this study can be low as it depends on the extraction of the animal samples, the fabrication of the phantom materials and the spectrophotometer configuration and calibration.

Conclusion

In conclusion, the results of this study demonstrated that both phantom materials have similar optical properties to mice and pigs' tissues, where the lowest differences are against the porcine model. It was found that the morphology, which can also be called behavior, trend, or geometry, of the phantom's spectra were very similar to the respective animal tissue comparator. Still there are differences in the amplitude of the absorption coefficients and the percentage of reflected light between the materials and the tissues, but the phantom's measurements are in between of the animal samples. Therefore, the proposed phantom materials are a good option for the development of a head phantom, that could work as the ideal platform in the evaluation of an optical multimodal sensor for TBI patients.

REFERENCES

[1] F. F. Jöbsis, "Noninvasive, Infrared Monitoring of Cerebral and Myocardial Oxygen Sufficiency and Circulatory Parameters," *Science (80-.).*, vol. 23, no. 4323, pp. 1264–1267, 1977.

[2] P. A. Roldan, Maria, Kyriacou, "Near-Infrared Spectroscopy (NIRS) in Traumatic Brain Injury (TBI)," *Sensors*, vol. 21, no. 1586, p. 30, 2021.

[3] A. Afshari *et al.*, "Cerebral oximetry performance testing with a 3D-printed vascular array phantom," *Biomed. Opt. Express*, vol. 10, no. 8, p. 3731, Aug. 2019.

[4] C. D. Kurth, H. Liuf, W. S. Thayers, and B. Chance, "A dynamic phantom brain model for near-infrared spectroscopy ," *Phys. Med. Biol.*, vol. 40, pp. 2079–2092, 1995.

[5] K. Kinoshita, "Traumatic brain injury: Pathophysiology for neurocritical care," *Journal of Intensive Care*, vol. 4, no. 1. BioMed Central Ltd., p. 10, 2016.

[6] A. I. R. Maas *et al.*, "The Lancet Neurology Commission Traumatic brain injury: integrated approaches to improve prevention, clinical care, and research Executive summary The Lancet Neurology Commission," *Lancet Neurol*, vol. 16, pp. 987–1048, 2017.

[7] A. Brazinova *et al.*, "Epidemiology of Traumatic Brain Injury in Europe: A Living Systematic Review," *J. Neurotrauma*, Dec. 2018.

[8] B. D. Greenwald, D. M. Burnett, and M. A. Miller, "Congenital and Acquired Brain Injury. 1. Brain Injury: Epidemiology and Pathophysiology," *Arch Phys Med Rehabil*, vol. 84, no. 1, 2003.

[9] M. Martin *et al.*, "Prediction of Early Intracranial Hypertension After Severe Traumatic Brain Injury: A Prospective Study," *World Neurosurg.*, vol. 127, pp. e1242–e1248, 2019.

[10] C. Sokoloff *et al.*, "Clinical Usefulness of Transcranial Doppler as a Screening Tool for Early Cerebral Hypoxic Episodes in Patients with Moderate and Severe Traumatic Brain Injury," *Neurocrit. Care*, 2019.

[11] A. T. Mazzeo and D. Gupta, "Monitoring the injured brain," *J. Neurosurg. Sci.*, vol. 62, no. 5, pp. 549–562, 2018.

[12] M. Roldan, T. Y. Abay, and P. A. Kyriacou, "Non-invasive techniques for multimodal monitoring in Traumatic Brain Injury (TBI): systematic review and meta-analysis," *J. Neurotrauma*, p. neu.2020.7266, Aug. 2020.

[13] A. Benninghaus, O. Balédent, A. Lokossou, C. Castelar, S. Leonhardt, and K. Radermacher, "Enhanced in vitro model of the CSF dynamics," *Fluids Barriers CNS*, vol. 16, no. 1, p. 11, Apr. 2019.

[14] S. Bottan, "In-vitro model of intracranial pressure and cerebrospinal fluid dynamics," 2013.

[15] D. H. Robbins and J. L. Wood, "Determination of mechanical properties of the bones of the skull," *Exp. Mech.*, vol. 9, no. 5, pp. 236–240, 1969.

[16] J. H. McElhaney, J. L. Fogle., J. W. Melvin, R. R. Haynes, V. L. Roberts, and N. M. Alem, "Mechanical properties of cranial sutures," *J. Biomech.*, vol. 23, no. 4, pp. 313–321, 1990.

[17] L. Falland-Cheung, J. N. Waddell, K. Chun Li, D. Tong, and P. Brunton, "Investigation of the elastic modulus, tensile and flexural strength of five skull simulant materials for impact testing of a forensic skin/skull/brain model," *J. Mech. Behav. Biomed. Mater.*, vol. 68, no. February, pp. 303–307, 2017.

[18] R. Vink, "Large animal models of traumatic brain injury," *J. Neurosci. Res.*, vol. 96, no. 4, 2017.

[19] OxiplexTS, "A non-invasive, real-time monitor of precise tissue oxygenation and hemoglobin concentration," *Newton Drive*, 2001. [Online]. Available: http://www.iss.com/biomedical/instruments/oxiplexTS.html. [Accessed: 24-Feb-2020].

[20] B. J. Clark, *UV Spectroscopy: Techniques, Instrumentation and Data Handling (Google eBook)*, 1st ed., vol. 4. London: Chapman & Hall, 1993.

[21] F. Bevilacqua, D. Piguet, P. Marquet, J. D. Gross, B. J. Tromberg, and C. Depeursinge, "In vivo local determination of tissue optical properties: applications to human brain," *Appl. Opt.*, vol. 38, no. 22, p. 4939, 1999.